Utilizing multilayer structures to enhance terahertz characterization of thin films ranging from aqueous solutions to histology slides

QIUSHUO SUN,[1] KAI LIU,[1] XUEQUAN CHEN,[1] XUDONG LIU,[2] A. I. HERNANDEZ-SERRANO,[3] EMMA PICKWELL-MACPHERSON[1,3,*]

[1]*Electronic Engineering Department, Chinese University of Hong Kong, Hong Kong*
[2]*National-Regional Key Technology Engineering Laboratory for Medical Ultrasound, Guangdong, Key Laboratory for Biomedical Measurements and Ultrasound Imaging, Department of Biomedical, Engineering, School of Medicine, Shenzhen University, Shenzhen 518060, China*
[3]*Physics Department, University of Warwick, Coventry, CV4 7AL, United Kingdom*

**Corresponding author: E.MacPherson@warwick.ac.uk*

Received XX Month XXXX; revised XX Month, XXXX; accepted XX Month XXXX; posted XX Month XXXX (Doc. ID XXXXX); published XX Month XXXX

We propose a multilayer geometry to characterize thin film samples in reflection terahertz time domain spectroscopy. Theory indicates that this geometry has higher sensitivity compared to ordinary transmission or reflection geometries when characterizing both low and high absorption samples. Pure water and water-ethanol mixtures are measured to verify the characterization accuracy of the proposed geometry and its capability to measure trace liquids. Paraffin-embedded oral cancer tissues are imaged to further show how the proposed geometry enhances the sensitivity for solid low-absorptive films.

http://dx.doi.org/10.1364/OL.99.099999

Terahertz (THz) material characterization techniques need to be developed properly for THz potential industry applications [1]. A wide range of THz potential biomedical applications are also being investigated [2]. The characterization of thin film (TF) samples, i.e. when the thickness of the sample is comparable with or much less than the wavelength of THz light, is not as straightforward as that for bulk samples. Conductive TF samples are difficult to characterize in ordinary transmission geometry because there is an insignificant reduction in the amplitude and phase shift of the signal that has passed through the sample. For example, a 300 nm thick $MAPbI_3$ perovskite only causes less than a 10% change in the wave intensity [3]. In low signal to noise ratio systems, it is difficult to track such minor spectral changes. The subtle phase shift also brings uncertainty in extracting optical properties. To avoid this issue, total internal reflection (TIR) spectroscopy has been proposed [4] and proved to enhance the THz responsivity of perovskites by a factor of 4 [3].

To characterize liquid TFs, the attenuated total reflection spectroscopy [5] is not applicable anymore as it requires the sample thickness to be larger than the penetration depth of the wave. Metamaterial sensing is able to detect small concentration changes in aqueous solutions with the usage of tiny amounts of samples [6], unfortunately it requires a complicated fabrication process and high resolution in the frequency domain to capture the frequency shift.

Additionally, an approach to enhance the THz response of low absorptive TFs is needed. Paraffin-embedded TF tissue samples are commonly used in THz biomedical studies because of their stability compared with fresh *ex vivo* tissue samples [2]. However, given the low contrast between the refractive indices and absorption coefficients of healthy and cancer tissue [7, 8], the discrimination between these two types of samples is very difficult in transmission geometry.

In this paper, we propose using a multilayer structure to characterize aqueous solutions and paraffin embedded tissues in reflection geometry. We derive equations from electromagnetic theory to demonstrate the high sensitivity of the proposed geometries. A paraffin embedded oral cancer tissue sample is imaged on a quartz window (no prism required): the contrast is enhanced by a factor of 5 compared to transmission geometry. Koch et al filed a patent in 2003 [9] for the idea that the refractive index of a solution can be measured very sensitively if it can represent one layer in a Bragg structure. Our work demonstrates this idea well; we use a prism to achieve the necessary angle of incidence for liquid measurements.

To compare the theoretical sensitivity between the geometries studied, we elaborate on the equations for each geometry in turn. Typically, in a transmission measurement, the solid TF samples are deposited onto a substrate whilst the liquid samples are sandwiched in between two substrates. For the single solid thin-film case, the transmitted THz electric fields from the sample and a bare substrate are measured as the sample and the reference signals. Their ratio can be written as below with the multi-reflection in the sample being considered [10]:

$$\frac{T_{sam}}{T_{ref}} = \frac{t_{air-sam} t_{sam-sub} P_{sam}(d_{sam}) P_{air}(-d_{sam})}{t_{air-sub}(1 + r_{air-sam} r_{sam-sub} P_{sam}^2(d_{sam}))} \quad (1)$$

where T_{sam} and T_{ref} are the transmitted sample and reference signals, d_{sam} is the thickness of the sample. The subscripts *air*, *sam* and *sub* represent the media of air, sample and substrate,

respectively. $P_{X1}(d) = \exp(\frac{-i\omega\tilde{n}_{X1}d}{c})$ calculates the phase propagation and amplitude attenuation in medium *X1* for a distance of *d*, where $\tilde{n}_{X1} = n_{X1} - ik_{X1}$ is the complex refractive index of the medium *X1*. Coefficients t_{X1-X2} and r_{X1-X2} are the transmission and reflection coefficients at the interface from media $X1$ to $X2$, calculated by Fresnel equations [10]. Similarly, we have derived the equation for the liquid case where two substrates are included (the reference here is the signal from the two substrates separated by a distance of the sample thickness):

$$\frac{T_{sam}}{T_{ref}} = \frac{t_{sub1-sam}t_{sam-sub2}P_{sam}(d_{sam})(1+r_{sub1-air}r_{air-sub2}P_{air}^2(d_{sam}))}{t_{sub1-air}t_{air-sub2}P_{air}(d_{sam})(1+r_{sub1-sam}r_{sam-sub2}P_{sam}^2(d_{sam}))} \quad (2)$$

where *sub1* and *sub2* indicate the substrates 1 and 2. For reflection spectroscopy, an imaging window is normally used to hold the sample. The equations to extract the permittivity of bulk materials have been given by Chen *et al* [11]. If the sample is a TF, the equation can be written as below [12]:

$$\frac{R_{sam}}{R_{ref}} = \frac{r_{win-sam} + r_{sam-top}P_{sam}^2(d_{sam}\cos\theta_{sam})}{r_{win-air}(1+r_{win-sam}r_{sam-top}P_{sam}^2(d_{sam}\cos\theta_{sam}))} \quad (3)$$

where R_{sam} and R_{ref} are the reflected sample and reference signals, θ_{sam} is the refracted angle in the sample, win and top represent the window and the medium on top of the sample. The reflection from the window to air is taken as a reference.

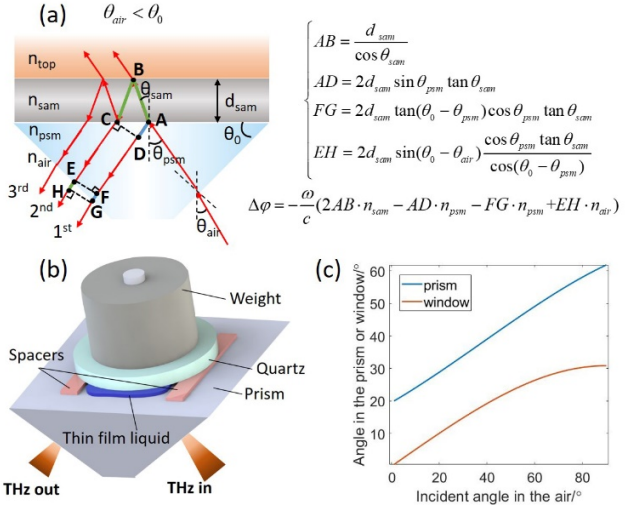

Fig. 1. (a) Illustration of the phase difference of the first and second reflections in the prism when $\theta_{air} < \theta_0$. The blue paths (AD and FG) indicate the distance that the first reflection travels more than the second reflection, the green paths (AB, BC and EH) indicate the distance that the second reflection travels more than the first reflection. $\Delta\varphi$ is the overall phase difference between two reflections. (b) Schematic diagram of TF liquid characterization measurements. (c) Calculated incident angles in the quartz prism (θ_0 =38°) and the quartz window as a function of incident angle in the air.

The incident angle in the window must be below the critical angle between quartz and air; larger angles can be achieved by using a prism. As shown in Fig. 1(a-b), we used a fused quartz dove prism with the top angle $\theta_0 = 38^\circ$. Fig. 1 (c) shows that the incident angle in the quartz prism (θ_{psm}) is larger than that in the quartz window and is a function of the incident angle in the air.

When a prism is used, the equations need to be modified to account for the phase difference, Δφ, caused by the prism. Fig. 1 (a) and Eqn (4) give the phase difference of the first and second internal reflections in the sample layer corresponding to the $\theta_{air} < \theta_0$ case. The $\theta_{air} > \theta_0$ case has the same expression after simplification.

$$\Delta\varphi = -\frac{\omega}{c}(2AB\cdot n_{sam} - AD\cdot n_{psm} - FG\cdot n_{psm} + EH\cdot n_{air}) \quad (4)$$

By substituting the expressions of *FG* and *EH* (shown in Fig. 1(a)) into Eqn (4), we see that the sum of the last two terms $-FG\cdot n_{psm} + EH\cdot n_{air}$ is zero. This results in the same expression as the window case, consequently Eqn (3) can be used to describe the multilayer reflection structure for both the window and the prism cases, by replacing $r_{win\text{-}air}$ and $r_{win\text{-}sam}$ with $r_{psm\text{-}air}$ and $r_{psm\text{-}sam}$. Defining the complex ratio between the sample and reference signals as $M = \frac{R_{sam}(\omega)}{R_{ref}(\omega)}$ in reflection or $M = \frac{T_{sam}(\omega)}{T_{ref}(\omega)}$ in transmission, we are able to calculate *M* at a specific frequency ω when a sample property $\tilde{n}_{sam}$ is given. This allows us to analyze the sensitivity of different geometries, as a geometry with a higher sensitivity gives a larger variation of *M* for the same amount of change in $\tilde{n}_{sam}$. It also indicates a better robustness, as the same amount of measurement error on *M* gives rise to a smaller influence on the characterized $\tilde{n}_{sam}$. Therefore, we calculate the resulting *M* value at 0.5 THz of water-ethanol mixtures with different ethanol volume fractions for different geometries. The window is made of z-cut quartz and the prism is made of fused quartz, for both cases the reflections are calculated for p-polarization. The sample properties of different volume fractions are characterized from the traditional bulk-reflection measurements. The relative change (RC) in the amplitude of *M* is calculated by Eqn (5) and shown in Fig. 2 (a), where $M_{V\%=0}$ is the complex ratio between the water and reference signals.

$$RC_{abs(M)} = \frac{abs(M) - abs(M_{V\%=0})}{abs(M_{V\%=0})} \times 100\% \quad (5)$$

In Fig. 2(a), the sandwich reflection geometry has a more significant change in the THz responsivity as the refractive index of the liquid changes, replacing the window with the prism increases the sensitivity in the amplitude further. The high sensitivity comes from the refractive index match between the two layers that surround the sample.

To evaluate the sensitivity on low-absorptive solid samples, such as paraffin-embedded tissue, we assume the refractive indices of the cancer and normal tissue are $n_c = 1.63 - 0.05i$ and $n_n = 1.56 - 0.03i$[8]. We consider using water as the top medium in the sandwich geometry to give better contact with the tissue. The percentage change of abs(*M*) by the cancer tissue was compared to that by the normal tissue, calculated by Eqn (5). Fig. 2(b) shows that the quartz window-sample-water setup can display the highest contrast between the normal and cancer tissue. In contrast, the transmission geometry only has less than 2% difference. Thus, we will show THz imaging results of oral cancer from sandwich reflection spectroscopy based on the window setup later.

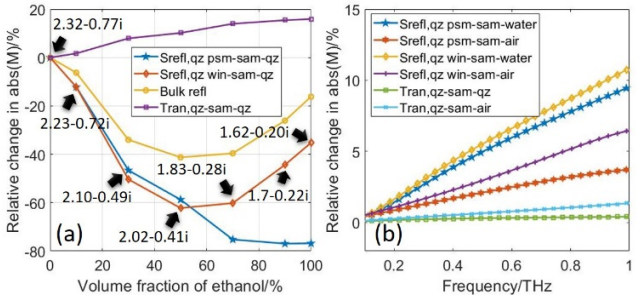

Fig. 2. (a) Calculated relative changes in the amplitude of M in different geometries at 0.5 THz, assuming sample thickness $d_{sam} = 25\mu m$, $\theta_{air} = 30°$, the top angle in the prism is 38°, the samples are water-ethanol mixture solutions with different volume fractions, the complex refractive indices of the samples are marked. Srefl is the proposed sandwich reflection geometry, calculated by Eqn (3), blue and orange curves correspond to the prism and window setups. Yellow and purple curves are bulk reflection and transmission setups, calculated by the equations in [11] and Eqn (2). (b) Percentage change of the amplitude of M by the cancer tissue compared to the normal tissue, assuming sample thickness $d_{sam} = 30\mu m, \theta_{air} = 30°$, both the window and the prism are made of quartz. The Srefl lines are calculated by Eqn (3), light green and light blue lines are calculated by Eqn (2) and Eqn (1), respectively.

The TF liquid measurements were conducted using the Terapulse 4000 from Teraview Ltd. The ethanol (≥99.8%) was from SIGMA-ALDRICH CO. The dove prism was made of fused quartz with a top angle of 38°. The top medium in the liquid measurements was a 2mm-thick fused quartz substrate. 25 μm Teflon spacers were sandwiched in the middle between the quartz prism and the substrate. The incident wave was p-polarized.

Fig. 1 (b) illustrates the schematic diagram of the TF spectroscopy setup for liquid characterization. There were three measurements that needed to be taken to extract the complex refractive index of the liquids: the signals from the bare prism, the TF sample being air and liquid, respectively. The signal from the bare prism was used as a reference, by combining with the TF air measurement, the accurate incident angle and thickness of the TF layer can be determined, and these were used to extract the permittivity of the sample. A weight (intensity of pressure 2.56 N/cm^2) was used to keep the thickness the same when switching from TF air to TF liquid.

The cancer tissue samples were formalin-fixed, paraffin-embedded (FFPE) blocks, provided by Nanjing Stomatological Hospital, Medical School of Nanjing University, and later were sectioned into 5 and 30 μm thick tissue slices. The 30 μm sections were mounted on z-cut quartz windows for THz imaging, the 5 μm sections were each mounted on a standard glass microscope slide and stained with hematoxylin and eosin (H&E) for pathology assessment.

The reflection and transmission tissue imaging were conducted using a fiber-coupled system from MENLO Ltd. and a free-space THz TDS system, respectively. The resolution of the image was 0.5 mm in both directions. In reflection geometry, the incident THz wave used was s-polarized and the tissue was sandwiched by quartz substrate (bottom) and water (top). All the imaging measurements were conducted with humidity at 4-5%. The THz imaging data were processed by Eqn (6):

$$\begin{cases} M_{mag} = \left| \dfrac{FFT(E_{sample}(t) \times WinFtn)}{FFT(E_{ref}(t) \times WinFtn)} \right| \\ M_{mag\_plot} = \dfrac{M_{mag}}{\max(M_{mag})} \end{cases} \quad (6)$$

$E_{sample}(t)$ is the time domain signal reflected/transmitted through the sample, $E_{ref}(t)$ is the signal reflected from quartz-water and transmitted through the quartz substrate in reflection and transmission geometries, respectively. The window function ($WinFtn$) applied is a standard Chebyshev window with 200 dB of sidelobe attenuation. The second equation is to normalize the amplitude on frequency domain for comparison.

The THz wave was totally reflected from the prism surface in the reference measurement. In order to accurately determine the incident angle (the prism might have a small tilted angle) and the slot thickness, we fitted the ratio between the TF air signal and the reference to the calculated theoretical value from Eqn (3). The calculated ratio was best fitted using 25 μm for the thickness and 30.5° for the incident angle.

The fitted angle and thickness were then used to extract the refractive index and absorption coefficient of water and compared them with the values in literature [13-16], as shown in Fig. 3. Both the refractive index and absorption coefficient match well with the reference. The error bars are the standard deviation from three measurements, and they are much smaller than the variation among the values from different references.

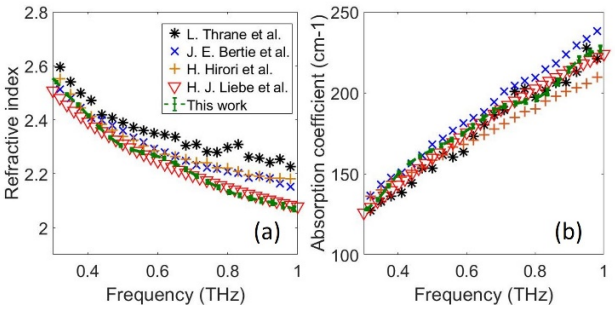

Fig. 3. Calculated refractive index and absorption coefficient of water compared to the literature values ([13-16]).

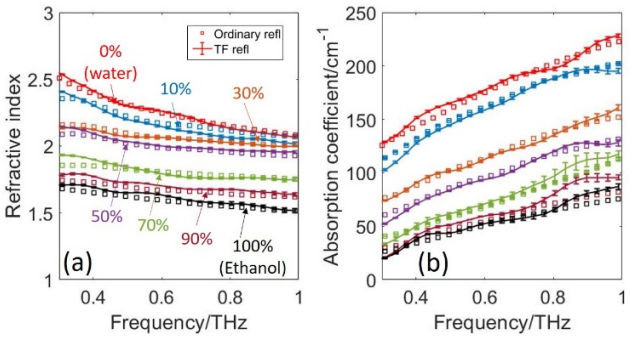

Fig. 4. Measured (a) refractive indices and (b) absorption coefficients of water-ethanol mixed solutions, the volume fraction of ethanol is from 0% to 100%. Squares are the results from the ordinary bulk reflection geometry, solid lines are the results from the proposed sandwich reflection measurement.

Similarly, we measured the properties of mixtures of water and ethanol and the results are shown in Fig. 4. In general, they are

very consistent with the results from the bulk reflection spectroscopy, whilst consuming much less sample volume.

The THz images of a paraffin-embedded oral cancer sample from transmission and sandwich reflection geometries are given in Fig. 5, as well as the visual and histology images. The normalized amplitude of M was calculated by Eqn (6) and plotted in Fig. 5(d-g). The transmission images (Fig. 5(d-e)) are slightly blurred because of the low contrast: at 1 THz the absolute value of M_{img} of the transmission image before normalization only varies between 0.94 and 1.06, this narrow dynamic range makes it difficult to discriminate between the cancer and normal tissues. However, using our proposed sandwich technique in reflection geometry, the dynamic range is significantly increased and the shape of the tissue in the THz reflection image at 0.5 THz (Fig. 5(f)) corresponds well with the dried tissue in Fig. 5(b), the black dashed circle area may indicate cancer as it is very distinct from the surrounding areas. To further check this, the histology image is given in Fig. 5(c). The cancer area is indicated by the black dashed line, and matches very well with the THz image at 1 THz (Fig. 5(f)). The color bars in Fig. 5(d-g) are the normalized amplitude of the processed waveforms as calculated by Eqn (6). From the ranges of the color bars, it is clear that the percentage changes in amplitude for Fig. 5f and Fig. 5g are much greater than for Fig. 5(d) and Fig. 5(e). From Eqn (5), we calculated that the contrast between the cancer and normal tissues was enhanced by over a factor of 5, by using the proposed multilayer reflection geometry compared to transmission geometry. To check if the high contrast in the reflection images was caused by the different water diffusion speeds going into the normal and cancer tissues, we imaged the tissue in reflection geometry repeatedly for 7 times within 2 hours interaction with water. However, no clear difference was observed. Consequently, we deduce that the high contrast mainly came from the geometry that we proposed, as calculated in Fig. 2(b).

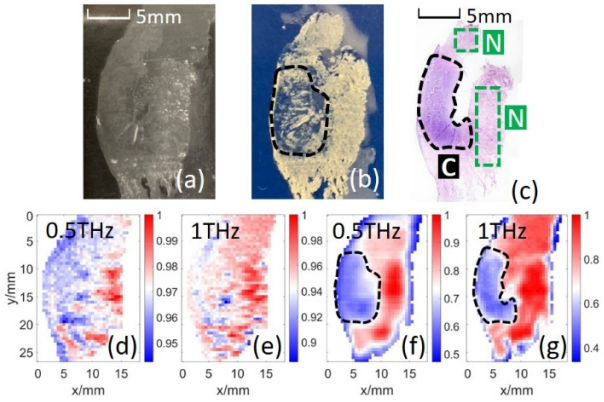

Fig. 5. Photographs of the paraffin-embedded oral cancer tissue (a) during the THz measurement, and (b) after drying, (c) histology image, the cancer area is marked with black dashed curve and the normal areas are marked with green dashed curves. (d-e) THz transmission spectroscopy images at 0.5 THz and 1 THz. (f-g) THz sandwich reflection spectroscopy images at 0.5 THz and 1 THz. The upper limit of the colormap scales of the THz images were all normalized to 1.

A THz multilayer reflection spectroscopy approach has been proposed to characterize TF liquids and enhance the imaging contrast of the tissue samples in this paper. In this technique, the thin-film sample is sandwiched in between two index-matching media to provide a greatly enhanced sensitivity. Thin-film liquids were measured to experimentally validate the theory, showing the ability of extracting accurate properties from a small amount of liquid by the proposed geometry. A paraffin-embedded oral tissue was also imaged by the proposed setup and transmission spectroscopy. The sandwich geometry gives a much better contrast and clear boundary between the cancerous and normal regions compared to transmission geometry. The greatly improved contrast achieved through this approach is a significant breakthrough for THz imaging, showing a promising potential in biomedical applications.

Funding. Hong Kong Research Grants Council (14201415); the Hong Kong Innovation and Technology Fund (ITS/371/16); National Natural Science Foundation of China (NSFC) (61805148). The Hong Kong PhD Fellowship Scheme (QS) and the Royal Society Wolfson Award (EPM).We are also grateful to Prof Hu Qingang, Prof Mou Yongbin and Dr Chen Sheng for their help with histopathology.

References

1. S. Dhillon, M. Vitiello, E. Linfield, A. Davies, M. C. Hoffmann, J. Booske, C. Paoloni, M. Gensch, P. Weightman, and G. Williams, J. Phys. D: Appl. Phys. **50**, 043001 (2017).
2. Q. Sun, Y. He, K. Liu, S. Fan, E. P. Parrott, and E. Pickwell-MacPherson, Quantitative imaging in medicine and surgery **7**, 345 (2017).
3. Q. Sun, X. Liu, J. Cao, R. I. Stantchev, Y. Zhou, X. Chen, E. P. Parrott, J. Lloyd-Hughes, N. Zhao, and E. Pickwell-MacPherson, J. Phys. Chem. C **122**, 17552-17558 (2018).
4. X. Liu, E. P. Parrott, B. S.-Y. Ung, and E. Pickwell-MacPherson, APL Photonics **1**, 076103 (2016).
5. M. Nagai, H. Yada, T. Arikawa, and K. Tanaka, International journal of infrared and millimeter waves **27**, 505-515 (2006).
6. T. Chen, S. Li, and H. Sun, Sensors **12**, 2742-2765 (2012).
7. K. Meng, T.-n. Chen, T. Chen, L.-g. Zhu, Q. Liu, Z. Li, F. Li, S.-c. Zhong, Z.-r. Li, and H. Feng, Journal of biomedical optics **19**, 077001 (2014).
8. T. Enatsu, H. Kitahara, K. Takano, and T. Nagashima, in *IRMMW-THz*(IEEE2007), pp. 557-558.
9. M. Koch, and P. Knobloch, "Verfahren zur bestimmung der beschaffenheit einer probe," (Technische Universitaet Braunschweig, 2003).
10. E. P. J. Parrott, "Applications of terahertz radiation," in *Department of Physics*(University of Cambridge, 2010).
11. X. Chen, E. P. Parrott, B. S.-Y. Ung, and E. Pickwell-MacPherson, IEEE Transactions on Terahertz Science and Technology **7**, 493-501 (2017).
12. J. McIntyre, and D. E. Aspnes, Surf. Sci. **24**, 417-434 (1971).
13. L. Thrane, R. H. Jacobsen, P. U. Jepsen, and S. Keiding, Chem. Phys. Lett. **240**, 330-333 (1995).
14. J. E. Bertie, and Z. Lan, Appl. Spectrosc. **50**, 1047-1057 (1996).
15. H. Hirori, K. Yamashita, M. Nagai, and K. Tanaka, Jpn. J. Appl. Phys. **43**, L1287 (2004).
16. H. J. Liebe, G. A. Hufford, and T. Manabe, International Journal of Infrared and Millimeter Waves **12**, 659-675 (1991).